The Astronomical Journal, 160:10 (6pp), 2020 July https://doi.org/10.3847/1538-3881/ab8f96

Lyα Observations of Comet C/2013 A1 (Siding Spring) Using MAVEN IUVS Echelle

Majd Mayyasi[1], John Clarke[1], Michael Combi[2], Nicolas Fougere[2], Eric Quemerais[3], Olga Katushkina[4], Dolon Bhattacharyya[5], Matteo Crismani[6], Justin Deighan[7], Sonal Jain[7], Nicholas Schneider[7], and Bruce Jakosky[7]
[1] Center for Space Physics, Boston University, MA, USA; majdm@bu.edu
[2] Climate and Space Sciences and Engineering, University of Michigan, MI, USA
[3] Laboratoire Atmospheres Milieux Observations Spatiales, Paris, France
[4] Russian Space Research Institute, Moscow, Russia
[5] University of Illinois, Urbana-Champaign, Il, USA
[6] Goddard Space Flight Center, MD, USA
[7] Laboratory for Atmospheric and Space Physics, CO, USA
Received 2019 December 7; revised 2020 April 29; accepted 2020 April 30; published 2020 June 10

Abstract

The close approach of comet C/2013 A1 (Siding Spring) to Mars in 2014 October provided a unique opportunity to observe a dynamically new Oort cloud comet with potential for interaction with a planet's atmosphere. The water-originating hydrogen coma of the comet extended to over 20 million km from the nucleus. Determining the properties of this coma contributes to characterizing the comet's water content and production rate. The present study analyzes a unique data set of high spectral resolution UV observations of comet C/2013 A1 Siding Spring measured by the Mars Atmosphere and Volatile Evolution spacecraft. The Siding Spring observations capture Lyα emissions from the Martian corona, the interplanetary medium, as well as the cometary H and D reservoirs. The isolated cometary spectra are analyzed to reveal a velocity distribution of H atoms that are consistent with model estimates of H_2O photodissociated H emissions and of OH photodissociated H emissions, Doppler shifted from the main comet H emission line center by 18 km s^{-1} and 8 km s^{-1}, respectively. The variations in comet H brightness with distance from the nucleus are used to constrain cometary water production to a rate of 0.5×10^{28} molecules s^{-1} at a time when Siding Spring was at 1.5 au, pre-perihelion.

Unified Astronomy Thesaurus concepts: Comets (280); Mars (1007); Ultraviolet sources (1741); Interplanetary medium (825)

1. Introduction

The discovery of Comet C/2013 A1 (Siding Spring), hereafter Siding Spring, caused community wide excitement as it was a dynamically new, active, ice-rich body from the Oort cloud that was on trajectory for a uniquely close encounter with a planet (McNaught et al. 2013; Farnocchia et al. 2014). Broadly encompassing observational campaigns for the comet included ground-based telescopes and balloon experiments as well as Earth, Moon, and Mars orbiting spacecraft with measurements that spanned multiple wavelengths made before, during, and after perihelion (e.g., Li et al. 2014; Bodewits et al. 2015; Stevenson et al. 2015; Andrienko et al. 2016; Opitom et al. 2016; Cheng et al. 2017; Magana et al. 2017).

The comet made its closest approach to Mars on 2014 October 19 at ~134,000 km (~40 Martian radii) from the planet center. The influx of cometary gas and dust particles on the Martian atmosphere produced numerous effects such as atmospheric heating (Restano et al. 2015), global ionospheric perturbations (Gurnett et al. 2015), enhanced particle interactions (Sánchez-Cano et al. 2018), indications of local magnetic field distortions (Espley et al. 2015), a significant meteor shower (Schneider et al. 2015; Crismani et al. 2018), and compositional changes to the atmosphere that lasted for several hours to few days after closest approach (Benna et al. 2015).

Constraining the water production rate of a comet is useful for determining its taxonomy, including compositional and dynamical properties (Combi et al. 2019). Water in the coma photodissociates and the chemical byproducts undergo additional chemical reactions to produce H atoms (Combi et al. 1998). Due to the close encounter of the comet with Mars, and the sensitivity of Mars' volatile atmosphere to the abundance of ambient hydrogen, an accurate determination of comet-originating hydrogen flux into the planetary atmosphere is critical for determining the effects of the comet passage on atmospheric composition, dynamics, and escape (Matta et al. 2013; Fox 2015).

Derivations of the comet water production rate during its closest approach to Mars ranged from ~1 to 4×10^{28} molecules s^{-1} (Gronoff et al. 2014; Kelley et al. 2014; Bodewits et al. 2015; Crismani et al. 2015). In this work, the first "up-close" high spectral resolution observations made of a comet from another planet are presented. Emissions from the comet obtained with this high resolution are uniquely resolved from other emissions and analyzed to constrain the water production rate that can be used for improved characterization of cometary chemical and kinetic properties.

2. Observations

The NASA Mars Atmosphere and Volatile Evolution (MAVEN) mission entered Mars' orbit on 2014 September, a month before comet Siding Spring's closest approach (Jakosky et al. 2015). The Imaging Ultraviolet Spectrograph (IUVS) instrument on board MAVEN includes a Far Ultraviolet detector for measuring hydrogen (H) Lyα emissions in low as well as high spectral resolution modes (McClintock et al. 2014). Due to the presence of an extended hydrogen corona at Mars that surrounds the MAVEN spacecraft orbit (Chaufray et al. 2008), and due to the orientation of the instrument line of sight during the comet viewing campaign, the IUVS observations of Siding Spring included contributions from cometary as

well as planetary and interplanetary Lyα emissions (Mayyasi et al. 2017a). Observations of comet Siding Spring made with the low-resolution mode of the IUVS instrument cannot disambiguate the multi-source contributions of H Lyα, and so, previous analyses included estimates for non-cometary emission contributions in the data (Crismani et al. 2015). The IUVS echelle channel, with a spectral resolution of 0.008 nm at Lyα, and a spectral sampling of 0.00071 nm pixel^{-1}, can resolve and uniquely constrain the numerous source contributions from Lyα emissions in the Siding Spring observations. The high spectral resolution echelle mode observations can further provide a unique velocity distribution for cometary-H atoms that, when paired with models, can elucidate chemical and kinetic properties of the comet.

IUVS echelle observations of Siding Spring were made on 2014 October 18 and include 72 images, each taken at 60 s integrations, beginning about 38 hr before closest approach. Siding Spring was moving toward Mars with a velocity of $\sim$56 km s^{-1} at the time of the observations and was between 7.8×10^6 and 7.5×10^6 km away from the planet. During the times of the observations used in this work, the instrument line of sight scanned various locations from the comet nucleus. The duration of the observations spanned about 1.25 hr between 03:56 and 05:14 UTC.

From the vantage of the echelle line of sight (LOS), the cometary H population was sufficiently Doppler shifted from the at-rest Martian H atoms to make emissions from the two populations fully resolvable. Interplanetary hydrogen (IPH) flows into the solar system at $\sim$23 km s^{-1} (Vincent et al. 2011), providing an added Doppler shift from the Mars emission. The echelle LOS for the Siding Spring observations (R.A.$_{SS} \sim 41°$, decl.$_{SS} \sim -14°$) was oriented between up- and cross-stream of the IPH flow (R.A.$_{IPH} \sim 252°$, decl.$_{IPH} \sim -15°$). The relatively small IPH Doppler shift ($\sim$5.6 km s^{-1}) produced a shoulder feature in the blue-ward wing of the Mars H emission spectrum that was not fully resolvable. A model of the IPH was therefore used to provide an initial estimate of the IPH brightness (Quémerais et al. 2008). Iterative fits for Mars H, IPH, and the comet H emissions were then made to separate the brightness of each component.

3. Results

The echelle LOS scanned the coma between $\sim$30,000 km and $\sim$185,000 km from the nucleus. Data from multiple images were coadded to improve signal to noise, by grouping observations according to the proximity of the LOS center to the comet nucleus at 4 reference locations: 30,000 km, 80,000 km, 120,000 km, and 185,000 km. The resulting spectra and fits to the H emissions from three components (Mars, Interplanetary, and Siding Spring) that have been co-added by proximity to the comet nucleus are shown in Figure 1.

The brightest contributions to the spectra from each distance from the comet nucleus are from solar resonant scattered Lyα from Mars' extended H corona, centered at 121.567 nm. The IPH peak emission is offset by $\sim$5.6 km s^{-1} blue-ward of the Mars H peak emission. The cometary components are sufficiently blueshifted off the Martian H line center to fully resolve the Lyα emissions. An initial estimate of a single bulk H population is assumed for the comet emissions.

The IPH emission is not fully resolvable from the Mars H emission. Therefore, iterative fitting was done to extract separate emission contributions from Mars H (red line), IPH (green line), and cometary H (blue line) in Figure 1. The Mars H line was fit using a curve determined by the IUVS echelle instrument line spread function (LSF) (Mayyasi et al. 2017a). The broader IPH and cometary H emissions were fit to a curve that convolves the LSF with a temperature-dependent Voigt profile to account for the diffuse emissions from those sources.

Initial estimates were used for: (1) the peak flux of Mars, using the LSF curve, (2) the peak flux of IPH, using the LSF curve, and (3) the temperature of the IPH emission, to be used to construct the Voigt profile for convolving with the LSF. These initial values were then varied incrementally over a plausible range. For each iteration, fit curves were compared with the data, and the best fit was obtained by minimizing χ^2 between the resulting curve and the data. Results from the best fit peak fluxes of the Mars and IPH emissions were used to integrate the best-fit curve over the wavelength range to produce a brightness value. The best fit curves are shown in Figure 1 and the resulting best fitting brightness values are listed in Table 1.

The IPH temperature that best fit the emissions in the spectra shown in Figure 1 was 22,000 K and is consistent with previous observations and models of the IPH (e.g., Clarke et al. 1998; Mayyasi et al. 2017a). The temperature that best fit the comet emissions was 10,500 K, and is a non-physical quantity used to include the multi-component velocity distribution from the different chemical pathways that produce cometary hydrogen (Combi et al. 1998, 2000). The best fit temperature is in good agreement with modeled estimates of the H coma kinetic temperatures at 1.5 au (Tenishev et al. 2008).

Deuterium (D) at Mars has a Lyα solar resonant scattering line at 121.535 nm. At the time of the comet measurements, Mars D emissions were bright enough to be captured by the IUVS echelle instrument but only when the LOS was pointed at or within $\sim$300 km of the sunlit disk (Mayyasi et al. 2017b). Deuterium atoms from the Martian upper atmosphere do not form as extended a corona as H atoms do due to their heavier mass. During the comet observations, the MAVEN spacecraft was $\sim$5000 km from the planet surface, and the instrument line of sight was pointing away from the planet disk. At such altitudes, the abundance of Martian D atoms along the instrument LOS is small enough that solar resonant scattering D Lyα emissions from these atoms are indistinguishable above the background noise level of the echelle detector (Mayyasi et al. 2017b). The contributions of Martian D Lyα emissions in the MAVEN echelle observations of Siding Spring are therefore considered undetectable.

The cometary spectra show a more structured and variable emission flux than that of Martian or interplanetary H, for observations made at increasing distance from the comet nucleus. This structure is attributed, in part, to the separate and non-thermalized H atoms produced with different velocities within the comae (Tenishev et al. 2008 and references therein). Removing the best-fit Martian and interplanetary contributions from the spectra of each reference location from the comet center highlights this variability more clearly as shown in Figure 2. The single-component best fit, as done for Figure 1, is made by convolving the instrument LSF with a Voigt profile. The multi-component fit is made by convolving the LSF with a velocity distribution (e.g., Combi et al. 2000) that represents the most probable branching pathways of cometary photo-dissociated H atoms.

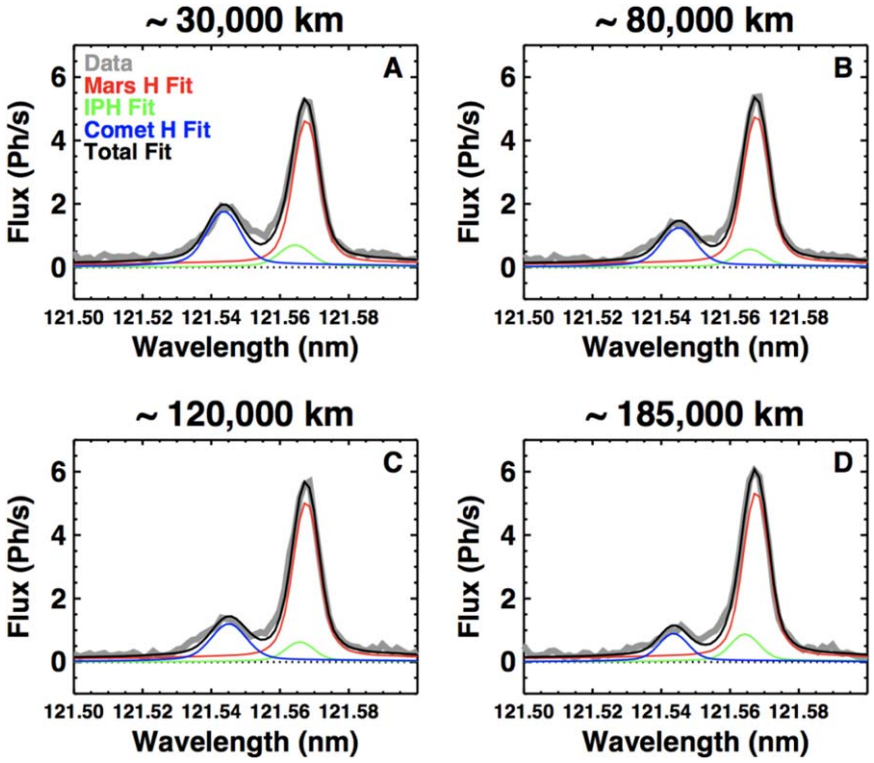

Figure 1. Co-added echelle spectra (gray) from (A) 30,000 km, (B) 80,000 km, (C) 120,000 km, and (D) 185,000 from the comet nucleus center. The contribution from solar resonant scattered Lyα from Mars' extended H corona, centered at 121.567 nm is best fit to a red line. The IPH component, offset by ~6 km s^{-1} blue-ward of the Mars H emission peak, is fit to a green line. The total cometary Lyα emission, offset by ~56 km s^{-1} from Mars H emission peak, is fit to a blue line. The sum of the fits to these three components is shown in black. A horizontal dotted line indicates the zero-flux level.

Table 1
Observed Brightness Values from the Four Comet-centric Reference Locations

LOS-Nucleus Distance ($\times 10^3$ km)	Mars H (kR)	IPH (kR)	Comet H (kR)	Comet D (kR)	Uncertainty (3σ(kR))	LOS R.A. (°)	LOS Decl. (°)
30 ± 17	1.64	0.257	0.625	0.060	0.109	41.2 ± 0.081	−14.6 ± 0.123
80 ± 17	1.68	0.199	0.452	0.041	0.106	41.3 ± 0.305	−14.6 ± 0.467
120 ± 17	1.78	0.210	0.456	0.022	0.091	41.7 ± 0.048	−13.9 ± 0.073
185 ± 17	1.89	0.295	0.321	0.046	0.121	41.9 ± 0.025	−13.6 ± 0.039

A significant H population is produced by the dissociation of OH (with a velocity distribution centered at 8 km s^{-1}). A secondary H population is produced by the dissociation of H_2O (with a velocity distribution centered at ~18 km s^{-1}), as well as a smaller distribution centered at 1 km s^{-1} (e.g., Combi et al. 2000). The radial extent of the H population from different photodissociation sources ranges from close to the nucleus, to ~10^7 km from the comet. At the time of the echelle measurements shown here, the MAVEN spacecraft was ~7.7×10^6 km from Siding Spring, and so was embedded in the outer shells of the extended cometary coma. The resulting Lyα contributions from comet Siding Spring's separate H populations reflect the line of sight proximity while capturing velocity distributions of ~8 and ~18 km s^{-1}. Additional modeling beyond the scope of this work would be required to more accurately represent the velocity distribution from within the coma at the spacecraft location.

As previously discussed, deuterium Lyα emissions from the atmosphere of Mars are not expected to contribute to the observed spectrum. However, the comet is expected to have a population of deuterium as well. D Lyα emissions from the comet are expected to be Doppler shifted blue-ward from ~121.535 nm to ~121.509 nm, as indicated by the thin red vertical line in Figure 2. Fitting the velocity distribution assumed for H atoms to the D cometary atoms is included in the multi-component fit (black lines in Figure 2). Both the H and D spectra vary with distance from the comet nucleus. These variations are indicative of variable kinetic properties as well as variable abundances of the parent atoms farther away from the comet center.

The brightness values of the multiple Lyα emissions are derived by integrating the respective best-fit spectra to within 4 FWHM of the emission peaks. The resulting brightness values for emissions of Martian H, interplanetary H, cometary H, cometary D are listed in Table 1. The uncertainty in these values due to detector noise (3σ) is also listed in Table 1 and applies to all the derived brightness values as their spectra are obtained from the same region and order on the echelle detector. The tabulated uncertainties take into consideration absolute, systematic, calibration source, and detector noise uncertainties of the MAVEN IUVS echelle channel (Mayyasi et al. 2017a).

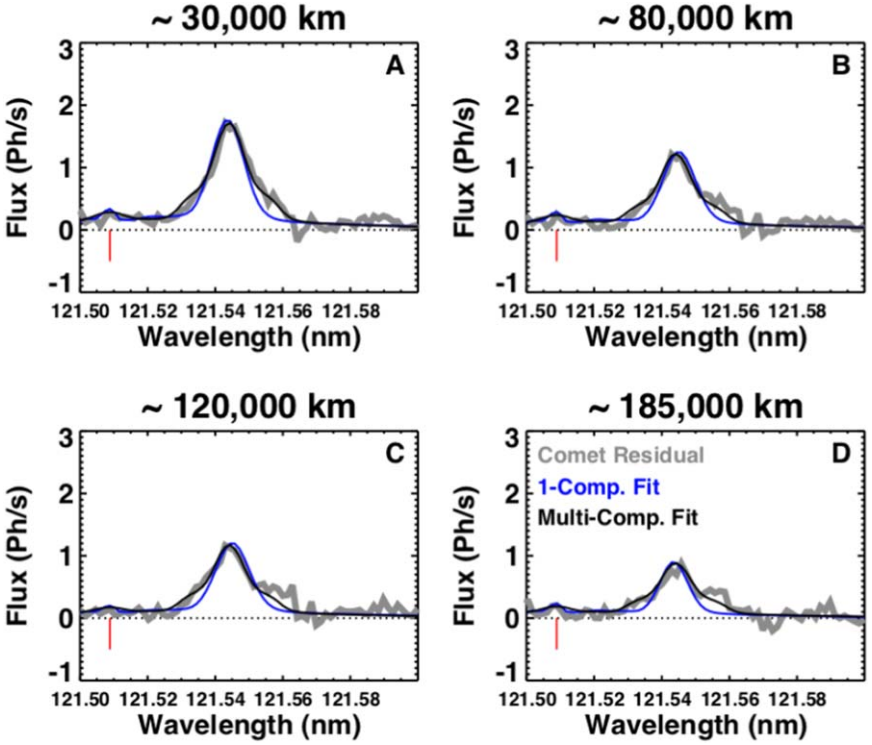

Figure 2. Comet residual H emission (gray) after removal of best-fit Mars H and IPH components at (A) 30,000 km, (B) 80,000 km, (C) 120,000 km, and (D) 185,000 from the comet nucleus center. The cometary spectra are fit using a single velocity population producing a diffuse Lyα emission (blue) as well as multi-velocity H and D components (black) using model estimates. A red vertical line at 121.511 nm denotes the spectral location of the Doppler shifted cometary D Lyα line emission center.

4. Discussion

At all distances from the comet nucleus, the derived D brightness is comparable to the 1σ uncertainty in the data due to detector noise, but smaller than the 3σ level of uncertainty that signifies a reliable detection. The D emission in Figure 2 is narrower than the multi-component curve used to fit the cometary H and scaled to D peak brightness. This is due to the heavier isotope being ejected with smaller speeds from HDO and OD photodissociation than similar reactions for H. The peak brightness for D Lyα emissions of an Oort Cloud comet is expected to be $\sim$2.5% that of H Lyα. For this family of comets, the D/H ratio lies in the range of $\sim 1.4 \times 10^{-4}$–6.5×10^{-4} (Hallis 2017). The ratio of peak brightness values of D and H emissions does not linearly translate into a ratio of the abundances provided by the D/H metric, due to variations in the optical properties along the line of sight that may or may not saturate an emission. The relative peak brightness of D to H Lyα emissions found here for Siding Spring is $\sim$10%. This relative brightness is significantly higher than that of a typical Oort Cloud comet, but the noise in the spectrum is too large to fully constrain the ratio of D to H in the observations analyzed here. Further interpretation of water evolution on the comet would require modeling beyond the scope of this work, however, if both D and H emissions are considered optically thin, then the ratio of emission brightness of D and H would be roughly proportional to the ratio of their densities. These observations place a constraint on the comet's D/H of $\leqslant$0.1, and pragmatically, would in all likelihood result in a value closer to that of other Oort cloud comets (Altwegg et al. 2015).

Derivations of the comet properties, including its water production rate, had been made prior to its perihelion pass, and included a value spanning 10^{27}–10^{29} molecules s^{-1} (e.g., Yelle et al. 2014). Pre-, at- and post-perihelion observations in the, UV, optical, and IR range have subsequently resulted in narrower estimates in the comet water production rate (Bodewits et al. 2015; Crismani et al. 2015; Cheng et al. 2017). MAVEN IUVS observations made with the low-resolution channel showed a water production rate of $\sim 10^{28}$ molecules s^{-1} (Crismani et al. 2015). That instrument, however, prohibits resolution of multiple contributions of H Lyα, and so model estimates were used to account for Martian and interplanetary H brightness. Swift UV–optical observations of the comet showed a water production rate of $\sim 1.5 \times 10^{28}$ molecules s^{-1}, assuming nonlinear variations in the availability of volatile active regions on the cometary surface (Bodewits et al. 2015). IR observations of the comet using a terrestrial balloon experiment gave a water production rate of $\sim 0.6 \times 10^{28}$ molecules s^{-1} using simplifying optical depth assumptions. This resulting production rate was then statistically adjusted to $\sim 10^{28}$ molecules s^{-1} (Cheng et al. 2017).

Previous MAVEN Lyα observations of comet Siding Spring did not have the resolution to separate the comet, interplanetary and Martian corona emissions, and so, assumptions were made to disentangle the individual components (Crismani et al. 2015). The high-resolution UV observations shown here have separated the individual comet Lyα contributions from those of interplanetary and Martian H, and can be considered to more accurately constrain comet models for the resulting water production rate. The brightness values in Siding Spring's H Lyα emissions, derived from the echelle observations, were used to constrain the production rate of cometary water by applying a Direct Simulation Monte-Carlo model (Fougere et al. 2016a, 2016b). This simulation uses a generic water production rate to produce an expected H Lyα brightness

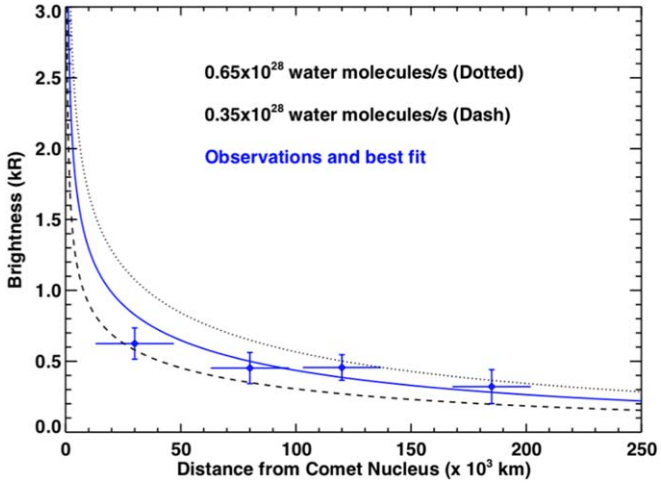

Figure 3. Comparison of model values of H Lyα brightness profiles with distance from the nucleus using water production rates of 0.65×10^{28} s^{-1} (dotted line), and 0.35×10^{28} s^{-1} (dashed line). Blue diamond symbols indicate the best-fit comet H brightness values (from Table 1) at 30,000, 80,000, 120,000 and 185,000 km from the center of the comet, yielding a best fit water production rate of 0.5×10^{28} s^{-1}. The vertical blue bars indicate the 3σ uncertainties in the brightness values. The horizontal blue bars indicate the distances from the comet nucleus over which data were co-added to produce a spectrum.

profile with distance from the comet nucleus. The water production rate scales linearly from its generic value with H Lyα emission brightness trends from the nucleus. Therefore, the observed brightness values of the comet at the four reference distances discussed in this work were used to determine the comet water production rate. Figure 3 shows the trends of H brightness as a function of distance from the comet. The resulting best-fit water production rate was 0.5×10^{28} H_2O molecules s^{-1}, and falls within the range of previous estimates. The observed brightness falls off more asymptotically than the model trends predict. This may be due to the sampling coverage of the echelle aperture size with respect to the cometary coma size that become more pronounced at larger distances from the nucleus.

There is abundant literature to describe the properties of comets and the numerous models to interpret the observed H emissions (e.g., Combi & Smyth 1988; Combi et al. 2019). However, few observations to date have been made at the resolution needed to distinguish the separate populations of H that defines and constrains the velocity distribution of photodissociated cometary water byproducts. To date, only one observation of this type has been published (Combi et al. 1998). The work presented here highlights the highest spectral resolution Lyα observations ever made of an active comet at such proximity to its nucleus, and the first such observations ever to be made from another planet.

5. Conclusion

High spectral resolution observations of comet Siding Spring made with the MAVEN IUVS echelle detector were analyzed to distinguish and quantify the numerous sources of Lyα emissions from four reference distances from the comet nucleus. The brightness of the Martian H coma and interplanetary H remained fairly constant throughout the comet observations, as expected for the relatively short observing time and relatively fixed LOS. Lyα flux from the comet varied with distance from the nucleus and showed a general asymptotic decrease in cometary H and D emissions with increasing distance from the comet center.

The MAVEN echelle instrumentation was designed with goals that include determining the D/H ratio in the upper atmosphere of Mars, for insights into water loss from the planet. Echelle observations of Siding Spring have been used to resolve the velocity distribution of cometary H emissions. The presentation of the unexpected opportunity to observe comets such as C/2013 A1, or 2I/Borisov (Opitom et al. 2019) may further demonstrate the capabilities of this instrument.

The authors would like to thank Jean-Loup Bertaux for useful discussions on instrument calibration. This work was funded, in part, by NASA contract 1000320450 from the University of Colorado to Boston University. The MAVEN data is available on the NASA Planetary Data System. The work presented here uses MAVEN IUVS level1a comet echelle data from orbit 106, modes 11 and 12, using version 13 release 2 data products.

ORCID iDs

Majd Mayyasi https://orcid.org/0000-0002-5663-602X
John Clarke https://orcid.org/0000-0002-8446-2645
Michael Combi https://orcid.org/0000-0002-9805-0078
Nicolas Fougere https://orcid.org/0000-0001-9626-004X
Olga Katushkina https://orcid.org/0000-0002-9378-1533

References

Altwegg, K., Balsiger, H., Bar-Nun, A., et al. 2015, Sci, 347, 1261952
Andrienko, Y., Golovin, A., Ivanova, A., et al. 2016, SoSyR, 50, 102
Benna, M., Mahaffy, P. R., Grebowsky, J. M., et al. 2015, GeoRL, 42, 4670
Bodewits, D., Kelley, M., Li, J.-Y., Farnham, T., & A'Hearn, M. 2015, ApJL, 802, L6
Chaufray, J.-Y., Bertaux, J.-L., Leblanc, F., & Quémerais, E. 2008, Icar, 195, 598
Cheng, A., Hibbitts, C., Espiritu, R., et al. 2017, Icar, 281, 404
Clarke, J. T., Lallement, R., Bertaux, J.-L., et al. 1998, ApJ, 499, 482
Combi, M., Brown, M., Feldman, P., et al. 1998, ApJ, 494, 816
Combi, M., Mäkinen, T., Bertaux, J.-L., Quemerais, E., & Ferron, S. 2019, Icar, 317, 610
Combi, M., Reinard, A., Bertaux, J.-L., Quemerais, E., & Mäkinen, T. 2000, Icar, 144, 191
Combi, M., & Smyth, W. 1988, ApJ, 327, 1044
Crismani, M., Schneider, N., Stevens, J., et al. 2018, JGRE, 123, 2613
Crismani, M. M. J., Schneider, N. M., Deighan, J. I., et al. 2015, GeoRL, 42, 8803
Espley, J., DiBraccio, G., Connerney, J., et al. 2015, GeoRL, 42, 8810
Farnocchia, D., Chesley, S., Chodas, P., et al. 2014, ApJ, 790, 114
Fougere, N., Altwegg, K., Berthelier, J. -J., et al. 2016a, A&A, 588, A134
Fougere, N., Altwegg, K., Berthelier, J. -J., et al. 2016b, MNRAS, 462, S156
Fox, J. 2015, Icar, 252, 366
Gronoff, G., Rahmati, A., Wedlund, C. S., et al. 2014, GeoRL, 41, 4844
Gurnett, D., Morgan, D., Persoon, A., et al. 2015, GeoRL, 42, 4745
Hallis, L. J. 2017, RSPTA, 375, 20150390
Jakosky, B. M., Lin, R. P., Grebowsky, J. M., et al. 2015, SSRv, 195, 3
Kelley, M., Farnham, T., Bodewits, D., Tricarico, P., & Farnocchia, D. 2014, ApJL, 792, L1
Li, J.-Y., Samarashiha, N., Kelley, M., et al. 2014, ApJL, 797, L8
Magana, L., Rutherford, K., Feldman, P., & Seifert, C. 2017, AAS, DPS Meeting, 49, 141.36
Matta, M., Withers, P., & Mendillo, M. 2013, JGRA, 118, 2681
Mayyasi, M., Clarke, J., Bhattacharyya, D., et al. 2017b, JGRA, 122, 10811
Mayyasi, M., Clarke, J., Quémerais, E., et al. 2017a, JGRA, 122, 2089
McClintock, W., Schneider, N. M., Holsclaw, G. M., et al. 2014, SSRv, 195, 75
McNaught, R. H., Sato, H., & Williams, G. V. 2013, CBET, 3368, 1
Opitom, C., Guilbert-Lepoutre, A., Jehin, E., et al. 2016, A&A, 589, A8

Opitom, C., Fitzsimmons, A., Jehin, E., et al. 2019, A&A, 631, L8
Quémerais, E., Izmodenov, V. V., Koutroumpa, D., & Malama, Y. 2008, A&A, 488, 351
Restano, M., Plaut, J., Campbell, B., et al. 2015, GeoRL, 42, 4663
Sánchez-Cano, B., Witasse, O., Lester, M., et al. 2018, JGRA, 123, 8778
Schneider, N., Deighan, J. I., Stewart, A. I. F., et al. 2015, GeoRL, 42, 4755
Stevenson, R., Bauer, J., Cutri, R., Mainzer, A., & Masci, F. 2015, ApJL, 798, L2
Tenishev, V., Combi, M., & Davidsson, B. 2008, ApJ, 685, 659
Vincent, F., Ben-Jaffel, L., & Harris, W. 2011, ApJ, 738, 135
Yelle, R., Mahieux, A., Morrison, S., Vuitton, V., & Hörst, S. 2014, Icar, 237, 202